NATIONAL RADIO ASTRONOMY OBSERVATORY
Charlottesville, Virginia

ELECTRONICS DIVISION TECHNICAL NOTE NO. 218

Dual-Mode Propagation in Triangular and Triple-Ridged Waveguides

Matthew A. Morgan

February 16, 2011

Dual-Mode Propagation in Triangular and Triple-Ridged Waveguides

Matthew A. Morgan
2/16/2011

I. Introduction

Every student of microwave engineering learns very early how to analyze the performance of hollow, metallic waveguides in terms of the doubly-infinite set of modes that can propagate within them. Intuition develops during the course of this study that the usefulness of any waveguide comes to an abrupt end when the first higher-order mode beyond the dominant one begins to propagate. In dual-polarization networks, such as orthomode transducers, this single dominant mode is replaced by two degenerate modes, but the presence of higher-order spurious modes can still be a serious impediment. They are tolerated only because the well-known dual-mode waveguides, having square and circular cross-sections, do not support enough bandwidth free of spurious modes to satisfy the requirements of modern radio astronomy receivers. Designers are forced to work around them by careful control of symmetry, aiming to avoid the excitation of these unwanted modes.

The quest for "perfect" symmetry is of course fraught with difficulties, especially when it comes into conflict with production schedules. Sharp resonances or suckouts from trapped high-order modes are a common occurrence, especially in cryogenic components with high Q-factors. By improving fabrication tolerance, one may suppress them – even visually eliminate them – but they must always be present to some degree.

Fortunately, square and circular waveguides are not the only dual-mode waveguides to choose from, nor are they even the simplest. Arguably, triangular waveguides are even more basic and fundamental then square waveguides, but to date they have been largely overlooked. Indeed, it is surprising how little-used triangular waveguides are, for we will soon see that they posses some unique properties. They occupy a singular position among simple, convex waveguides for having the broadest bandwidth over which they support exactly two degenerate modes and no others. Nor can their relative obscurity be blamed on the need for advanced CAD tools to analyze them, for relatively simple closed-form solutions describing them do, in fact, exist [1]-[3] – simpler, some might say, than for circular waveguides. They even have less loss than their circular or square counterparts over identical bandwidths.

In this memo, we explore the characteristics of triangular waveguides and other forms which exhibit three-fold symmetry. In Section II, we focus on the convex, hollow waveguides described above. In Section III, we further exploit the properties of three-fold symmetry by demonstrating a coaxial structure which over an arbitrary bandwidth supports only two degenerate modes in addition to the TEM mode. Finally, in section IV, we will illustrate how a triple-ridged waveguide can achieve theoretically unlimited bandwidth as a dual-mode waveguide, unencumbered by spurious higher-order modes, while the more common quad-ridged waveguides cannot.

II. Convex Hollow Waveguides

Before considering the broadband performance of triangular waveguides, it is worth first discussing the behavior and appearance of the dominant mode. Various representations of this mode are shown in Fig. 1 for different polarization angles. Those shown at the far left, labeled with polarization angles of 0° and 90°, are those that would couple directly into the horizontal and vertical linear polarizations from the feed. These field patterns, however, while mathematically orthogonal, are clearly not identical, making it difficult to visualize them as belonging to the same mode. (Perhaps it is this violation of our intuition that has kept triangular waveguides in relative obscurity for so long.) Nonetheless, these field patterns have the same cutoff frequency, the same impedance, the same dispersion characteristics, even the same loss per unit length. To convince ourselves, we need only recognize that the field patterns in the top row are simply linear combinations of the field patterns in the bottom row, and vice versa. Thus, we see that the dominant-mode ensemble in triangular waveguide may be drawn in linear polarizations as a pair of orthogonal but non-identical modes (such as those labeled 0° and 90°), or as a trio of identical but non-orthogonal modes (0°, 120°, and 240°).

If further proof is needed that the triangular waveguide can support propagating modes in both polarizations without a physical bias for either one, then it helps to realize that there is one final decomposition of the dominant mode that comprises field patterns which are both orthogonal *and* identical. Specifically, these are circularly-polarized waves, wherein the instantaneous field pattern rotates sequentially through all those shown in Fig. 1 in either the clockwise or counter-clockwise direction.
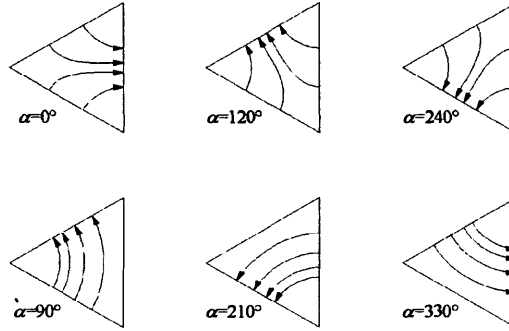
Fig. 1. Several representations of the TE_{11} mode in triangular waveguide.

We now turn our attention to the cutoff frequencies of higher-order modes. Three forms of simple, convex, dual-mode waveguides are shown at the top of Fig. 2. The triangular waveguide is indicated at the left edge, the circular waveguide in the middle, and the square waveguide at the right. The graph below the diagram shows the cutoff frequencies of the first ten modes that propagate in these waveguides, normalized to that of the dominant mode, for which the physical scaling factor is plotted in the bottom graph. The horizontal axis of both graphs corresponds to the radius, r, of the inside corners of the triangular and square waveguides, normalized to the diameter of the inscribed circle, a. Note that when $a=2r$ for either polygonal waveguide, the cross-section becomes circular. This highlights the relationship between the modes in the three waveguides as well as providing practical information for designing real waveguides that are cut by conventional end-mills.

Transverse-electric (TE) modes are shown with solid lines, transverse-magnetic (TM) modes with dashed lines. Parallel lines indicate a degenerate mode. The modes are labeled using the convention for circular waveguides, wherein the indices correspond to cycles in polar coordinates. For consistency, this labeling will be used throughout this document, regardless of the actual shape of the waveguide. Thus, what is normally referred to in square waveguides as the TE_{10} or TE_{01} mode, but is known in circular waveguides as TE_{11}, as well as the dominant mode of the triangular waveguide, will herein be referred to as TE_{11}, and so on.

Several things are noteworthy about the plot. First, we see that the geometry of the square waveguide breaks up the degeneracy of the TE_{m1} modes where m is even – consider TE_{21} for example, which is degenerate on the left side of the plot, but splits into two as the waveguide becomes more square on the right side of the plot. Similarly, the triangular waveguide breaks up the degeneracy of TE_{m1} modes where m is odd, such as the TE_{31} mode. In general, the same observations could be made about polygonal waveguides with even- and odd-numbers of sides, respectively – except for the TE_{11} mode, which is always degenerate for any regular polygonal waveguide.

More important, however, is that the higher-order modes all shift upward as you trace the curves to the left. The first higher-order modes level off at $\sqrt{3}$ above the dominant mode, compared to $\sqrt{2}$ for the square waveguide. T his shows that the spurious-mode-free bandwidth of the triangular waveguide is more than 20% larger than that of the square waveguide, and more than 30% larger than for the circular waveguide. The bandwidth in both polygonal waveguides is limited simultaneously by two parasitic modes, and the TM_{01} mode is a limiting factor common to all three.

Now, we consider how the loss of these waveguides compares. A great deal depends on what one assumes regarding the size of the waveguide that would be used in each case. If all three were sized to have identical cutoff frequencies in the dominant mode, than the triangular waveguide would be at a disadvantage because it is being compared to other waveguides which cannot even be used at the higher frequencies where its loss is the best. If, on the other hand, we restrict our comparison to frequency ranges that all three waveguides can support, then the triangular waveguide has a significant advantage in that it can be made much larger, and in waveguides more metal is typically associated with less loss. This is illustrated in Fig. 3, where the loss is plotted for each of the three guides, and the frequency axis is normalized to the cutoff of the first higher-order mode, f_{c2}. This ensures that the loss for each waveguide is plotted only for that range over which it has exclusively dual-mode operation. The vertical axis is normalized also to the conductivity of the metal walls. Not only does the triangular waveguide achieve the lowest loss, it will also be subject to less dispersion within overlapping frequencies because it has a lower cutoff than the other two waveguides.
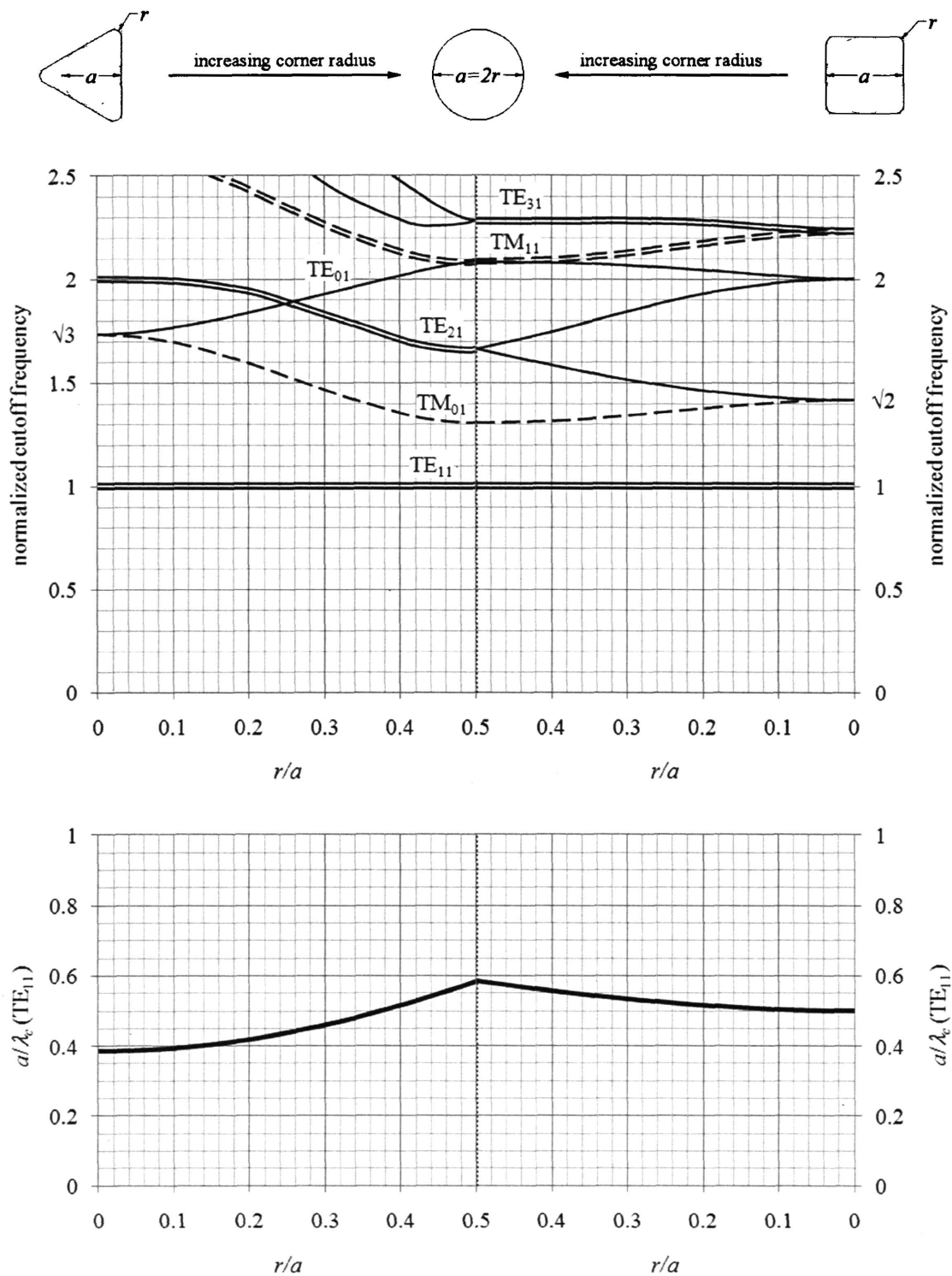
Fig. 2. Mode plot (above) and dominant mode scaling factor (below) for a hollow metallic waveguide, gradually varying from a triangular waveguide at the left to circular in the middle and finally a square waveguide at the right. TE and TM mode indices correspond to polar coordinates typical for circular waveguides.
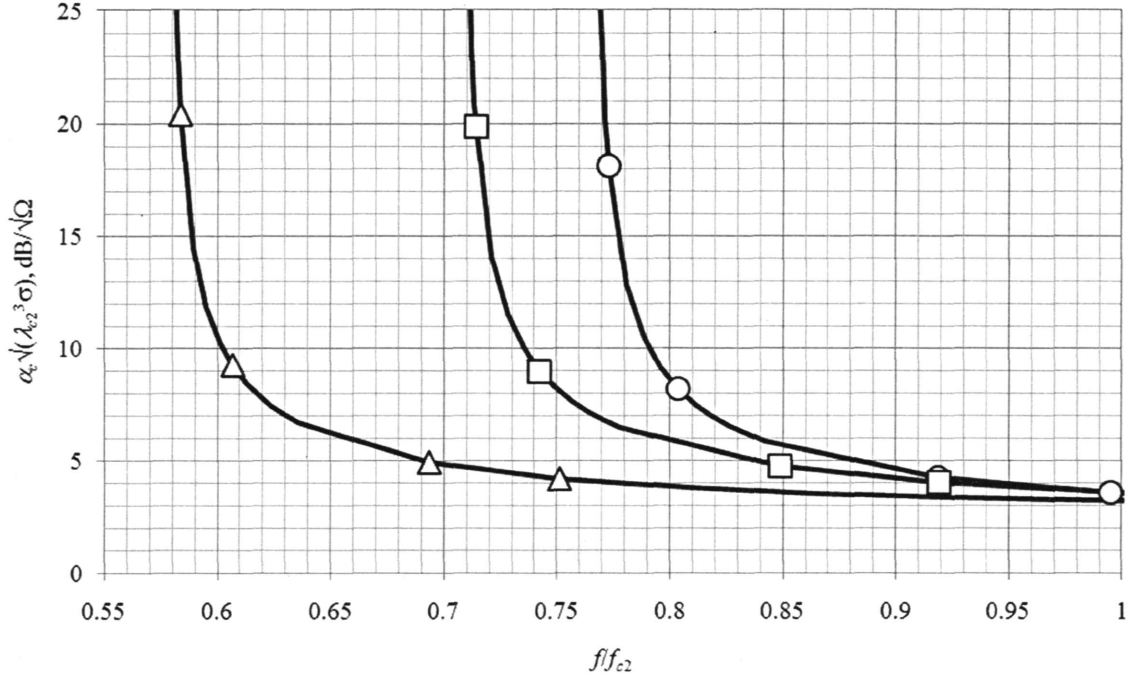
Fig. 3. Simulated loss per unit length for triangular, circular, and square waveguides (indicated by the shape of the markers). The frequency axis is normalized to the cutoff of the first spurious mode. The loss is normalized according to the wavelength of this cutoff, as well as for the bulk conductivity of the metal walls.

III. Coaxial Waveguides

The next general class of waveguide we wish to consider will be referred to as coaxial waveguides. These are waveguides with nested inner and outer conductors, starting with the familiar coaxial transmission lines where both conductors have circular boundaries. Although the common use of "coax" is almost exclusively limited to single-mode applications, for this analysis we will consider them also as dual-mode waveguides. The presence of the TEM mode, however, can not be ignored. As discussed earlier in this report, one must ensure that it does not become trapped – or equivalently, that it is terminated somehow inside the structure. In fact, we will find that this additional mode has some interesting practical uses, which will be discussed in more detail in Section V.

A plot of the first ten modes and TE_{11} scaling factor for circular coax is shown in Fig. 4. (Interestingly, in this configuration we encounter a triple-degeneracy involving the TM_{11} and TE_{01} modes.) At the far left, the diameter of the inner conductor becomes infinitesimally small. With the exception of the TEM mode, the configuration of modes at this extreme is exactly the same as the circular waveguide at the center of Fig. 2. As the inner conductor grows, however, the higher-order modes quickly diverge. The center conductor is especially effective at suppressing transverse-magnetic modes such as TM_{01}, but at the cost of the added TEM mode which has a very similar field pattern. The TE_{m1} modes, on the other hand, all approach a relative cutoff frequency of m. This can be understood as the space between the inner and outer conductors narrows to a circular slit, and each mode simply turns on as the circumference of this slit becomes an integer multiple of the free-space wavelength. Unfortunately, this means that circular coax is fundamentally limited (for dual-mode purposes) to an octave bandwidth.

But what happens if we again introduce the three-fold symmetry described in Section II? The result is triangular coax, for which the mode plot and scale factor is shown in Fig. 5. The intercepts at the left, for which the inner conductor vanishes, are the same as those for the triangular waveguide. But as the inner conductor grows in size, all other modes except for TEM and TE_{11} diverge to infinity.

The importance of this result cannot be overstated. In a field where troublesome higher-order modes are tolerated only because the bandwidth is needed, we find that a minor change in the shape of the waveguide boundary increases its potential spurious-mode-free bandwidth from one octave to infinity. The limiting harmonic behavior
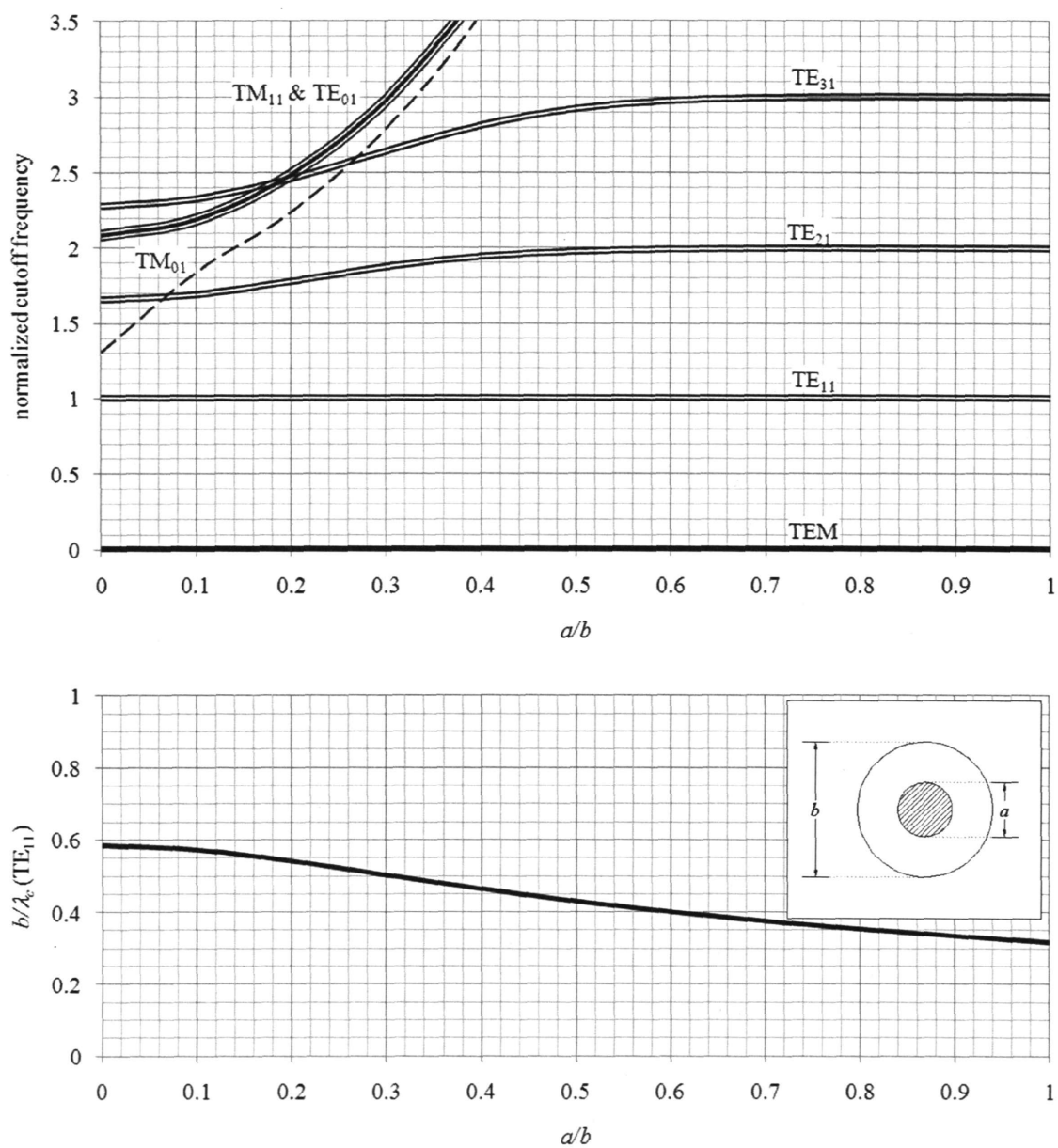
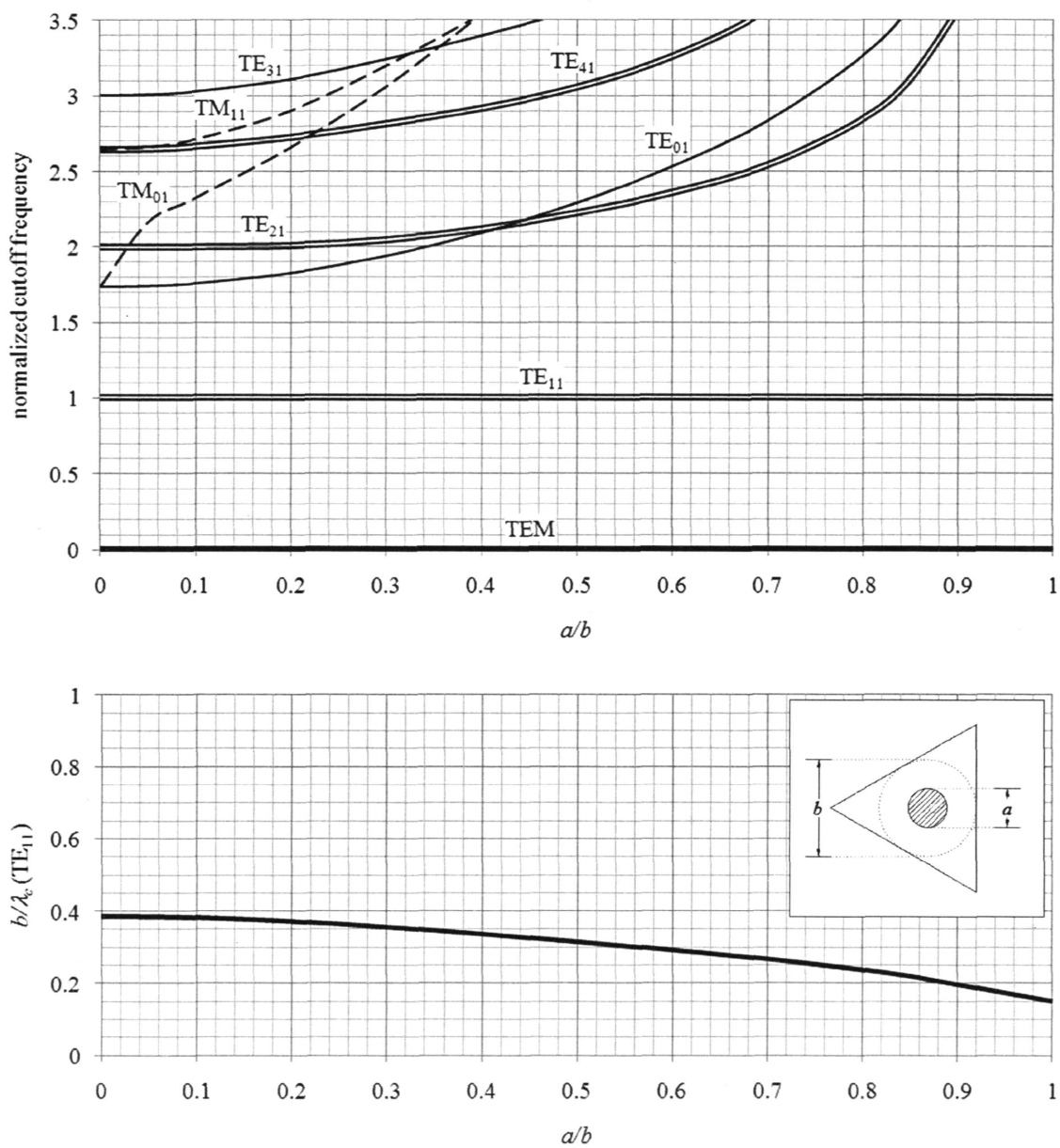Fig. 4. Mode plot (above) and scaling factor (below) for a circular coaxial waveguide.

Fig. 5. Mode plot (above) and scaling factor (below) for a triangular coaxial waveguide.

of the TE_{m1} modes observed before with circular coax did not occur. To understand why, we defer to the discussion of ridged waveguides in the following section. For now, we will only state without proof that a *squared* coaxial waveguide would again be limited in bandwidth, just as the circular coax was, and just as any other polygonal coax line would be. The mode-divergent behavior exhibited here is unique to triangular geometries.

IV. Ridged Waveguides

In order to push beyond an octave of bandwidth without the presence of the TEM mode typical of coaxial structures, we must look to ridged waveguides. A relative of the well-known double-ridge waveguides for broad bandwidth in single-mode applications, the quad-ridge waveguide shown in Fig. 6 is the familiar building block of the so-called Quad-Ridge OMT. Although Quad-Ridge OMTs are known for their broadband performance, they too are not immune to the fabrication difficulties that lead to trapped high-order modes and suckouts in the passband. Arguably, it is an attempt to avoid the excitation of these modes that leads to the long geometric taper that determines their size, along with the obvious impedance-matching requirements (for if it were not for the presence of other modes, impedance-matching could be accomplished in more compact ways with abrupt transitions). A glance at the mode diagram for this waveguide illustrates the problem. Although most of the modes diverge as the gap size decreases, the lower TE_{21} mode becomes tangentially degenerate to the TE_{11} mode. The risk exists for minor imperfections in manufacturing to cause the TE_{11} and TE_{21} modes to couple, and then for the TE_{21} mode to become trapped in the narrow part of the taper, leading to a suckout.

Note that the circular outer boundary and the ridge width parameter, w/b, were chosen for convenience as a good compromise between bandwidth and loss while avoiding extremes in feature size. Other choices would result in slightly different mode diagrams, but the overall character remains the same. It will soon become clear – even intuitive – that the limiting bandwidth is solely a function of the number of ridges and has nothing to do with these minor details.

First, however, let us examine for comparison the mode plot for a triple-ridged circular waveguide, as shown in Fig. 7. A different ridge-width parameter was found to be a good compromise between bandwidth and loss in this case, but again the overall character of the plot is not dependent on this detail. The critical feature is that none of the other modes in this waveguide stay near the TE_{11} mode cutoff as the gap size decreases. Unlike the quad-ridge waveguide, every other mode, including TE_{21}, diverges to infinity, leaving TE_{11} to propagate alone and giving this waveguide virtually unlimited bandwidth as a dual-mode component.

Perhaps surprisingly, there is an intuitive explanation for this behavior. As the gap size in any ridged waveguide decreases, the electromagnetic fields become increasingly concentrated in the center, and the currents all flow predominantly in the tips of the ridges. In the limit, then, the remaining "unused" metal may be removed entirely, resulting in an N-wire transmission line as an approximate model for the lowest-order modes in an N-ridge waveguide. This approximation is illustrated in Fig. 8. The number of TEM modes such a structure can support is simply N-1 (the number of degrees of freedom in assigning currents to the wires while maintaining a DC balance). Therefore, a quad-ridge waveguide must propagate three low-order modes in the limit, while the triple-ridge waveguide propagates only two.

A similar model can explain the behavior of the triangular coax we discussed in the previous section. As the center conductor grows, the fields concentrate in the ever-shrinking gap between this conductor and the sides of the outer triangle. The far corners of the triangle become "infinitely" far away in comparison, and the guide may be approximated by a four-wire transmission line with one wire in the middle. Thus, in the limit, it supports only three independent modes – the TEM mode and the two linear modes.

Naturally, unlimited bandwidth comes at a cost. The losses in a triple-ridge waveguide for a number of gap size parameters are plotted in Fig. 9. Although different in shape, the loss for 1.7:1 bandwidth in triple-ridge waveguide (a/b=0.6) is very nearly the same as it was for the triangular waveguide shown in Fig. 3. However, as the bandwidth increases (which is evident from the upturn in the loss at the low end), the average loss over the band also increases.

V. Analysis of Example Orthomode Transducers

In order to illustrate the value of spurious-mode-free operation and of the waveguide structures presented above, we will analyze the performance of two real orthomode transducers (OMTs) in this context. The first is a conventional Bøifot-Junction OMT designed for Band 6 (211-275 GHz) of the Atacama Large Millimeter Array (ALMA) radio telescope. This was chosen as a case study because of the author's experience with the production of this OMT (and consequently with its shortcomings). A model of the OMT and the narrow portion of the feedhorn is shown in Fig. 10. The mode plot for this OMT over the specified signal path is shown in Fig. 11.
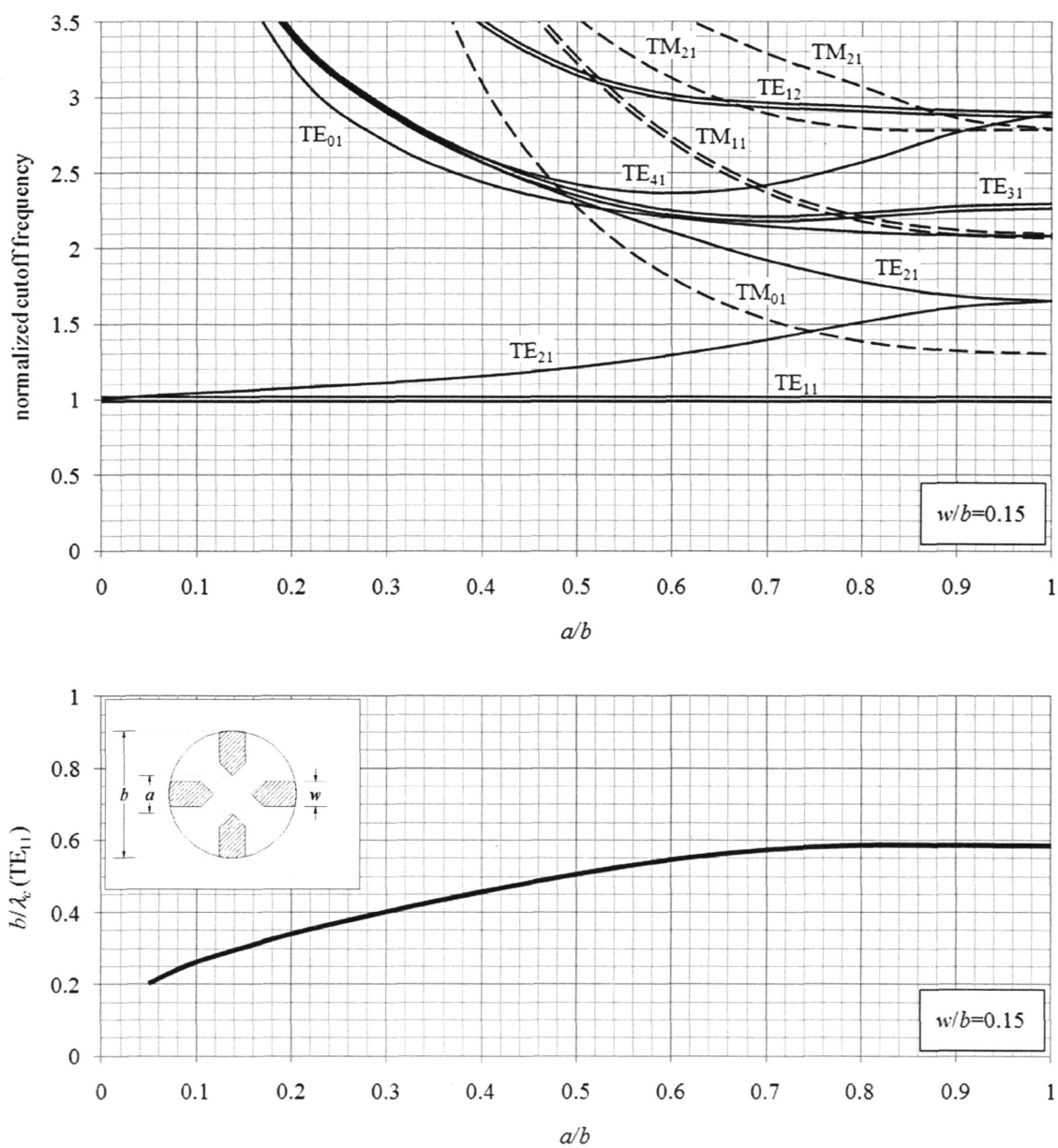
Fig. 6. Mode plot (above) and scaling factor (below) for a quad-ridged circular waveguide.
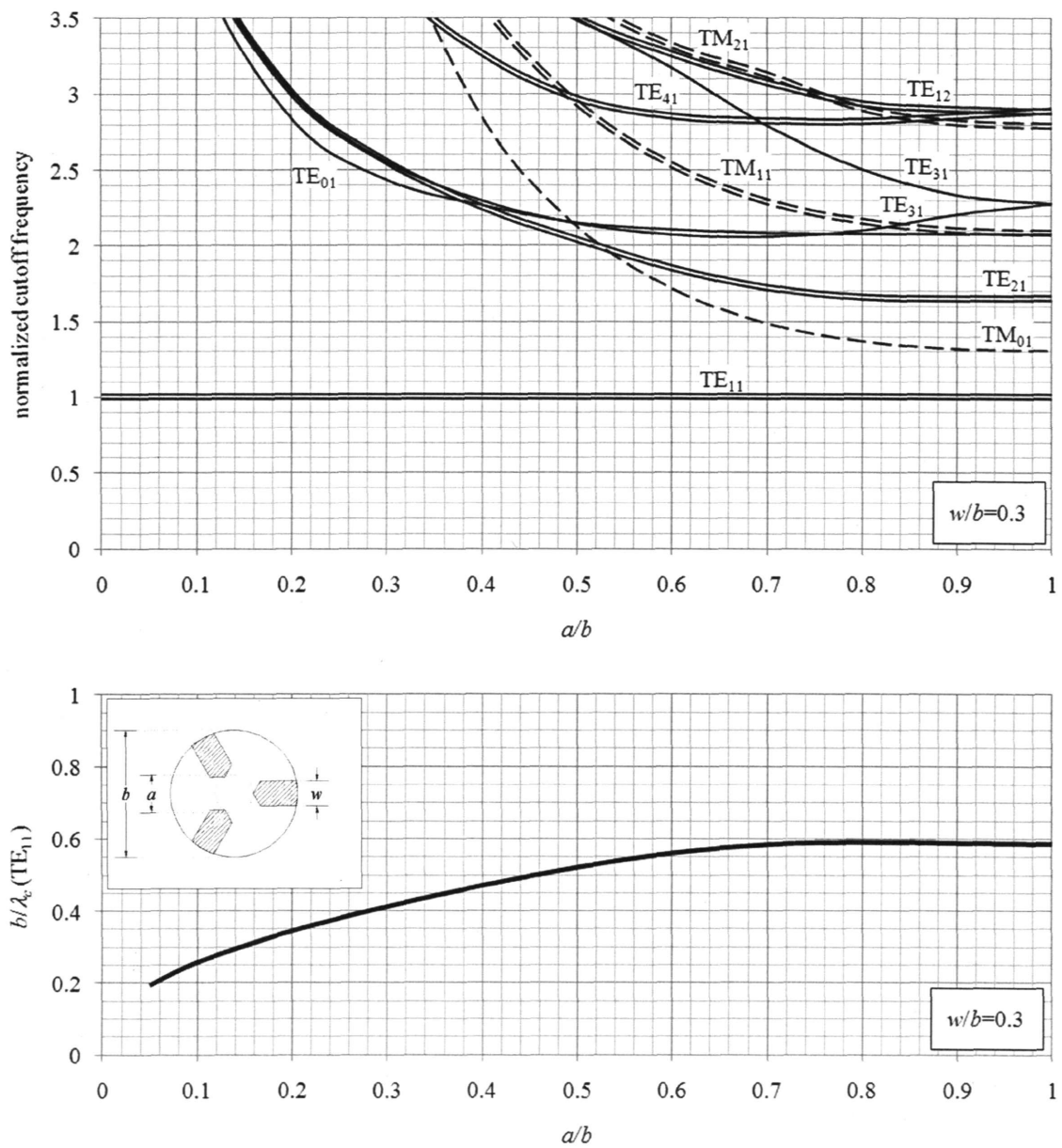
Fig. 7. Mode plot (above) and scaling factor (below) for triple-ridged circular waveguide.

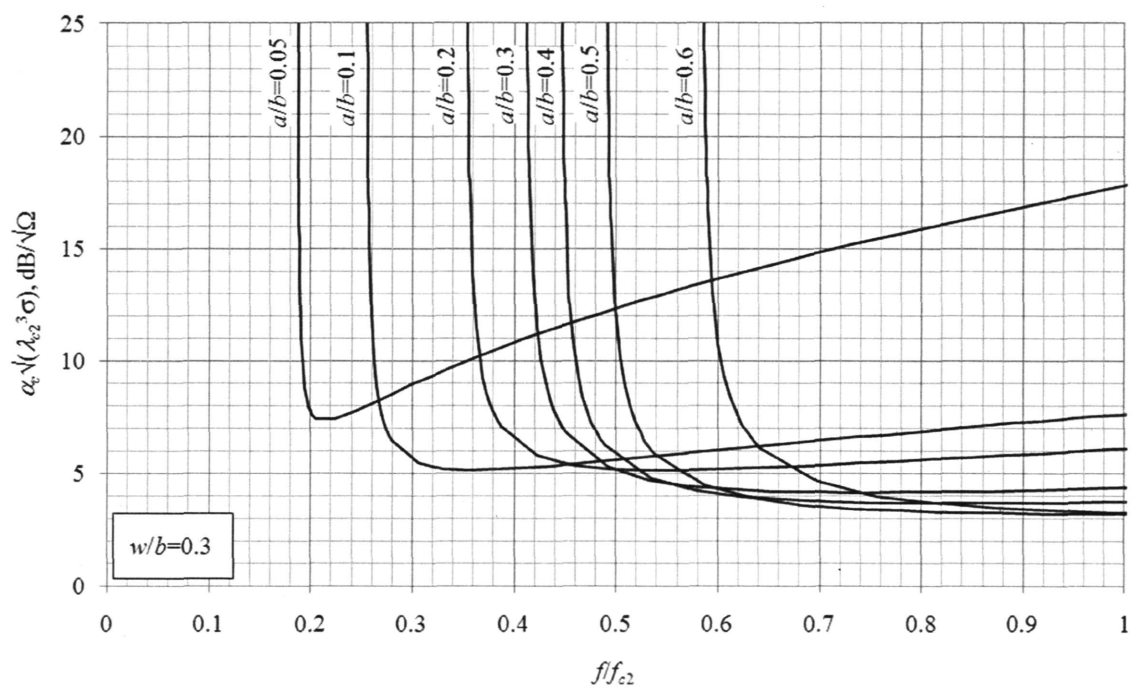Fig. 8. *N*-wire model for the low-order modes in ridged waveguides.

Fig. 9. Attenuation constant for triple-ridge waveguide with *w/b*=0.3. All curves are plotted over the spurious-mode-free bandwidth of the waveguide.
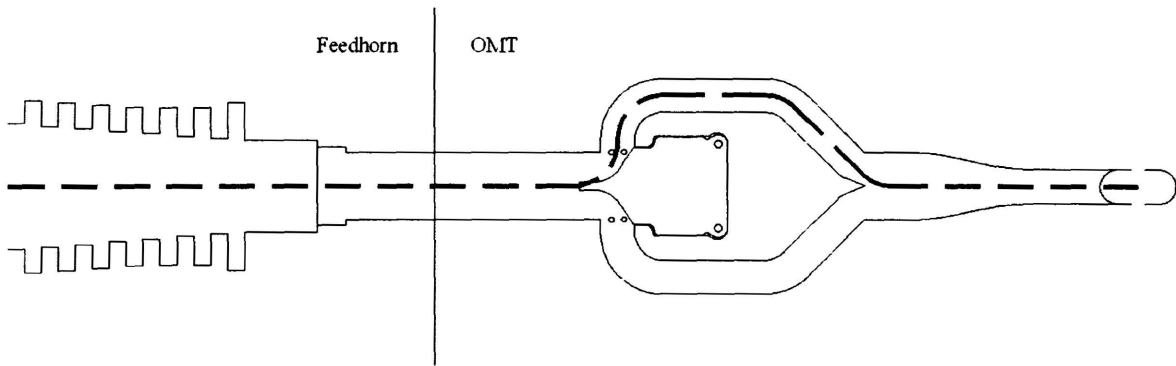
Fig. 10. Model of the dual-mode sections of the ALMA Band 6 corrugated feedhorn and orthomode transducer (OMT). The mode plot below was calculated for the signal path shown with the dashed line.
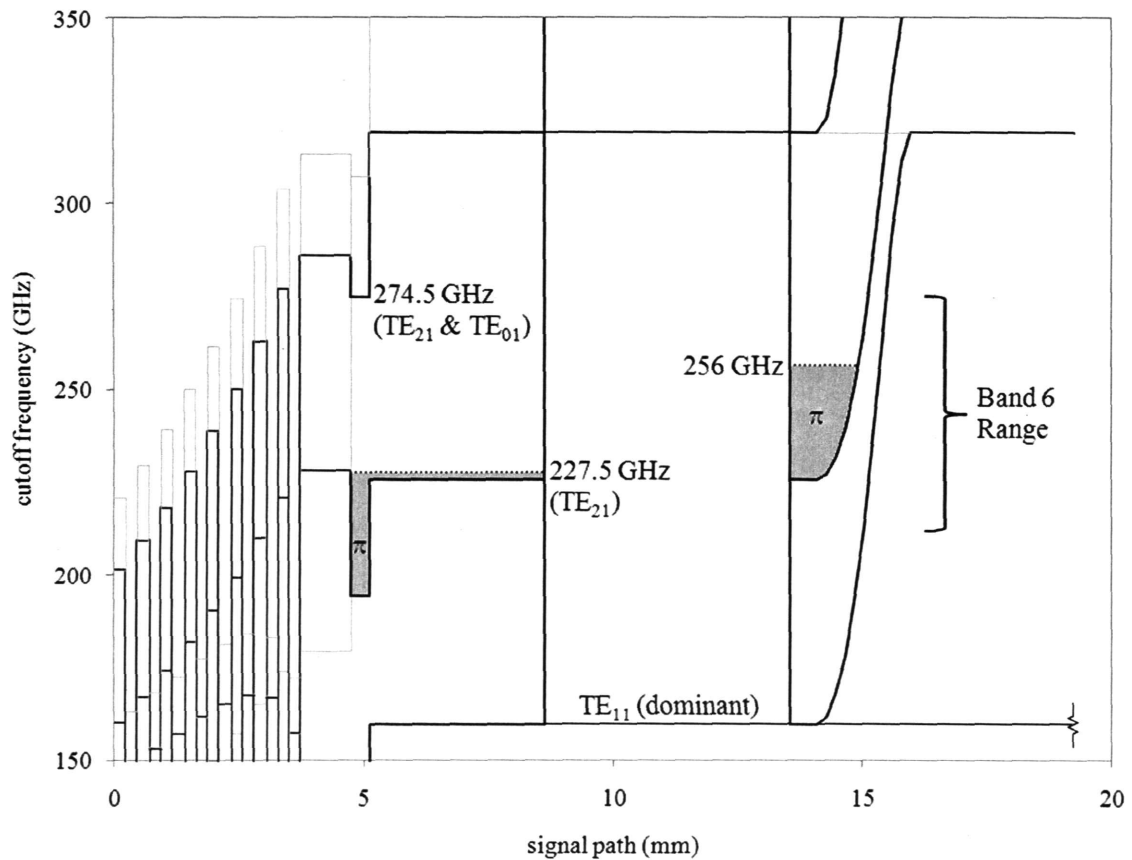

Fig. 11. Mode plot for the ALMA Band 6 feedhorn and orthomode transducer. Spurious-mode cutoff "wells" lead to resonances at 227.5 GHz and 256 GHz, while another at 274.5 GHz leads to poor cross-polarization at the top of the band. The resistor symbol at the bottom-right corner indicates that the dominant TE_{11} mode is terminated at the output of the OMT.

Several issues are immediately evident from this plot. First, the passband is contaminated by not just one, but several spurious modes that cut on and off at varying frequencies in different parts of the OMT. These modes and their cutoffs were identified during the design phase [4], however no action was taken to mitigate the risk they presented other than to assume that symmetry would avoid their excitation. Not so, unfortunately. Manufacturing tolerance may allow one to get away with that assumption at centimeter-wavelengths (from which this OMT design was scaled), but this is much more difficult at the submillimeter wavelengths at which the Band 6 design is being used. Given that asymmetry always exists at some level, the next important question to ask is how they will affect the OMT performance. As long as they remain un-trapped, then the excitation of these modes represent a graceful degradation of signal-to-noise ratio, cross-polarization performance, and possibly beam pattern efficiency. If the mode is trapped and resonant, however, the degradation is not graceful, but immediate. It commonly results in a gain suckout associated with a spike in receiver noise and phase instability. Trapped modes are indicated in the mode plot by cutoff "wells" where the cutoff of a particular mode reaches a minimum. The electrical phase in this well may be calculated from knowledge of the cutoff frequencies as

$$\theta(f) = \int_{x_1}^{x_2} \beta(x)dx = \int_{x_1}^{x_2} \left(\sqrt{k^2 - k_c^2(x)}\right)dx = \frac{2\pi}{c} \int_{x_1}^{x_2} f_c(x)\left(\sqrt{\left(\frac{f}{f_c(x)}\right)^2 - 1}\right)dx \qquad (1)$$

where $f_c(x)$ is the cutoff frequency at position x in the waveguide, and the well extends from x_1 to x_2. If the well is deep enough and/or long enough, then at some frequency the electrical length becomes π radians and the trapped mode becomes resonant. This may be represented graphically by shading in the bottom of the well as indicated in Fig. 11. The high-water level of the shaded region then is the point at which the mode resonates. This occurs in the Band 6 design twice, at 227.5 GHz and 256 GHz, and indeed both of these resonances have been observed in ALMA production receivers. The resonance at 227.5 GHz is most insidious, because it bridges across the feedhorn-OMT interface, and likely would never appear in standalone tests on either one.

In addition, an even higher-order mode turns on at 274 GHz in an impedance-matching section of the feedhorn. It is worth noting that this occurs directly at the interface between the square and circular regions of the feed, where the cutting of the mandrel switches from a lathe to a milling machine. The axial alignment of this transformer to the circular sections is thus subject to more error than are the circular corrugations to each other. The well is too shallow and narrow for this mode to be resonant so no suckouts should occur (and none have been reported), however conversion into this mode may account for marked degradation in cross-polarization performance frequently observed at this frequency. The periodic wells in the corrugated section of the feedhorn to the left are likewise too narrow to create suckouts, and as these are all cut in the same pass on a numerically controlled lathe, the concentricity of the corrugations is far better controlled than it is for the square transformer described above, however flexure of the mandrel after machining, but prior to electroforming, was a concern for this very reason.

Even more frustrating than the presence of these problems is the knowledge of how avoidable they would be if it was not too late to change the design. The lower-TE_{21} well at $x=5$ mm is barely deep enough to support a resonance. A 10 micron change (<0.8%) to the diameter of the circular throat of the feedhorn, one that could easily be absorbed into the design without compromising the dominant mode, would have eliminated the 227.5 GHz suckout completely. A comparable decrease in the dimensions of the square transformer would push the upper-TE_{21} cutoff from 274 GHz out of band to 277 GHz. Similarly, the 256 GHz resonance could be eliminated entirely by tapering the side-arm rectangular waveguides to half-height prior to combining them. These points illustrate the power of this kind of analysis in avoiding the problems associated with trapped modes. It is highly likely that if a plot of this type had been generated during the design phase, these minor modifications would have been implemented before construction ever began.

As a counter-example, let us examine another orthomode transducer designed for research and development purposes at S-Band (1.7-2.6 GHz) which uses the triangular and tri-coaxial waveguides described in this memo. A model of the interior of the OMT is shown in Fig. 12, and the mode plot is in Fig. 13. Right away, we see that the OMT is totally free of spurious modes throughout its passband, despite having 17% wider bandwidth than the Band 6 OMT. The TM_{01} mode is present at 2.1 GHz and above, however, in the circular waveguide which is part of the feedhorn to which this OMT will be connected. Although exact dimensions of the full feedhorn were not available at the time of this writing, it is unlikely that the feedhorn traps this mode.

The primary technical challenge in implementing an OMT with triangular geometries is how to couple into the two orthogonal polarizations efficiently without cross-coupling them. The solution is to extract not two orthogonal polarizations, but three identical ones as described earlier and shown in Fig. 1. A demonstration of this technique has
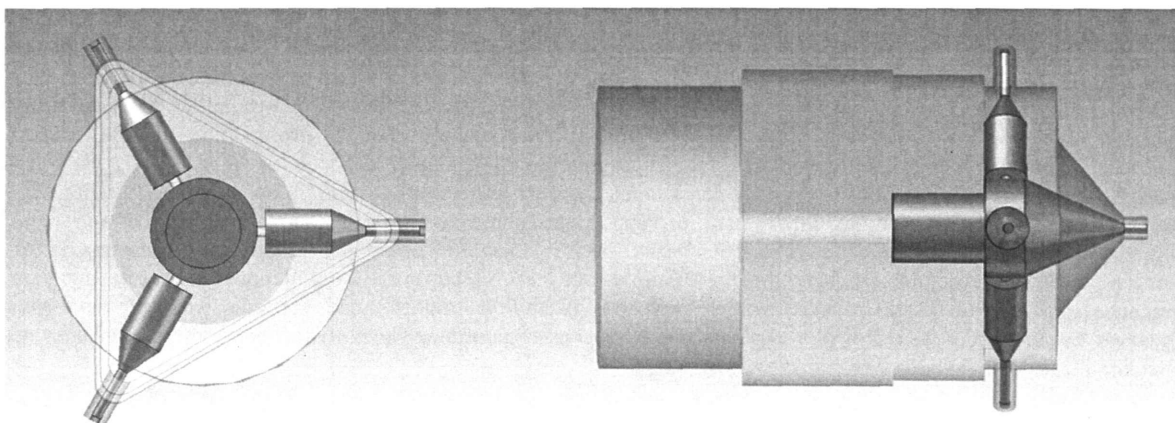
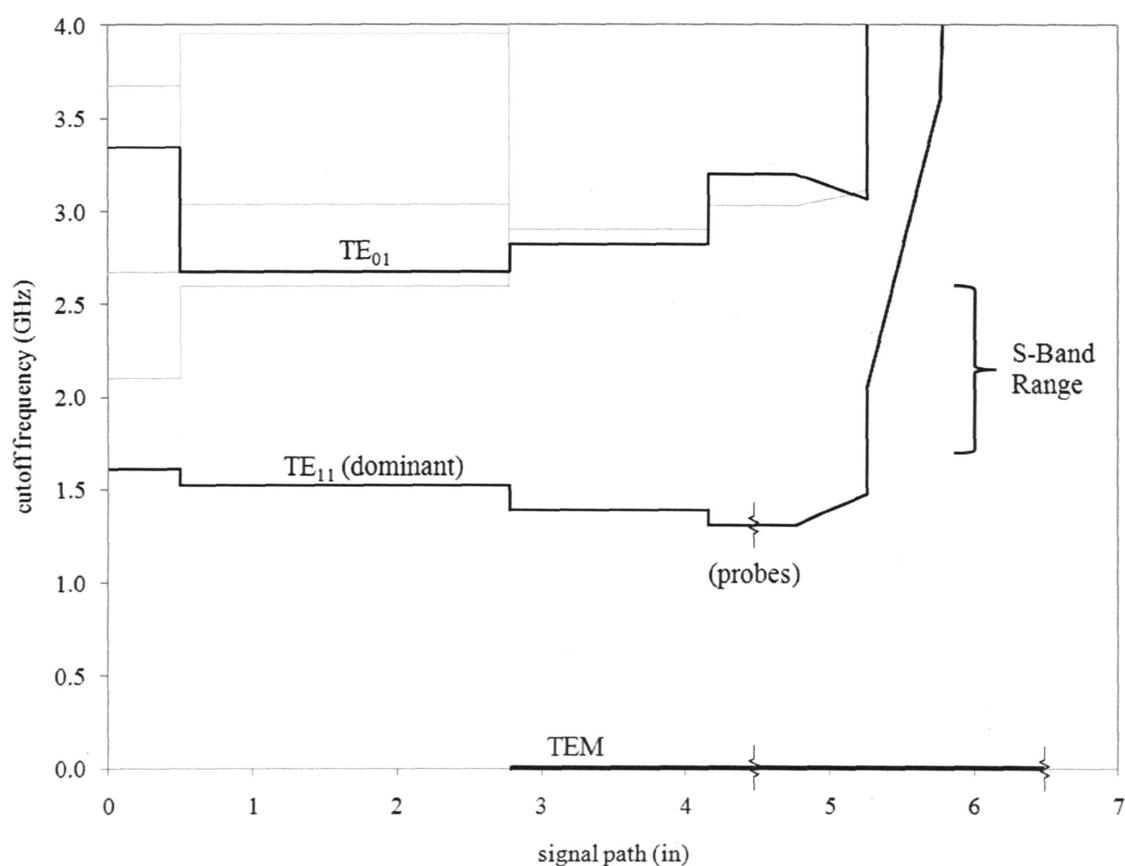Fig. 12. Model of the S-Band research orthomode transducer using triangular- and tri-coaxial waveguide.

Fig. 13. Mode plot of the S-Band research orthomode transducer, which is free of spurious modes throughout its operating range (though the TM_{01} mode is present in the circular feedhorn to which it will be connected). The cutoff well in the dominant TE_{11} mode does not lead to a resonance because the signal is captured by the probes that extend into the waveguide.

already been presented [5]. In contrast to that publication, the new OMT shown in Fig. 12 adds a coaxial reference port. The TEM mode, far from an inconvenience, was added intentionally for the injection of calibration signals into the active part of the receiver. This avoids the insertion loss normally associated with calibration couplers in front of the cryogenic amplifiers. It would also provide a loss-free means for coupling the local oscillator into a Schottky or SIS-Mixer front-end at higher frequencies, or an RF pilot tone for direct monitoring and correction of the receiver's $1/f$ gain fluctuations.

To push beyond the bandwidth of this example, one must switch over to the triple-ridged structure shown in Fig. 7. However, the conventional circular corrugated feedhorn in this case becomes a severe limitation. A better solution would be to extend the triple-ridged structure into the flare of the feedhorn itself, opening the door for almost any bandwidth desired from a closed-waveguide structure, subject to the practical constraints of insertion loss and broadband impedance-matching.

Conclusions

A comparative study of the mode content in various polygonal, coaxial, and ridged waveguides has been presented. In each of these categories, waveguides having triangular or three-fold symmetry were shown to possess unique characteristics that make them unsurpassed as dual-mode waveguides with broadband, spurious-mode-free operation. The value of this metric was illustrated by examining the modal properties of two real-world OMTs, the first using conventional square and circular waveguides, and the second using the triangular and tri-coaxial waveguides. Special emphasis was placed on quickly identifying trapped and resonant modes from the mode plots alone so they can be avoided in future OMT designs.

References

[1] V. Komarov, "Eigenmodes of regular polygonal waveguides," *Journal of Infrared, Millimeter- and Terahertz Waves*, vol. 32, pp. 40-46, 2011.

[2] K. Milton and J. Schwinger, *Electromagnetic Radiation: Variational Methods, Waveguides, and Accelerators*, ch. 7, Springer, 2006.

[3] M. Iskander and M. Hamid, "Analysis of triangular waveguides of arbitrary dimensions," *Archiv fuer Elektronik und Uebertragungstechnik*, vol. 28, pp. 455-461, November 1974.

[4] E. Wollack, W. Grammer, and J. Kingsley, "The Bøifot Orthomode Junction," *ALMA Memo Series*, no. 425, May 2002.

[5] M. Morgan, J. Fisher, and T. Boyd, "Compact Orthomode Transducers Using Digital Polarization Synthesis," *IEEE Trans. Microwave Theory Tech.*, vol. 58, no. 12, pp. 3666-3676, December 2010.